Broad-band Synthetic Aperture Sonar

Michael P. Hayes and Peter T. Gough

(*Invited Paper*)

Abstract—Most sonars, even chirped-pulse sonars, are narrow band in that their modulated bandwidth is a fraction of the carrier frequency. In this paper we look at the effects of a broad-band signal on the performance of a side-scan synthetic aperture sonar, including details on the necessary spatial sampling and resolution trade-offs. The mathematical description of the echo signals and the consequent image reconstruction algorithms are first shown for a step-and-go scenario that ignores the Doppler effect. Later, the extra modifications for the Doppler effect are introduced with some discussion of their probable impact.

Simulated echoes and image reconstructions on hypothetical targets show the limiting performance and some of the effects of narrow-band reconstruction approximations on broad-band signals. For comparison purposes a few real images are presented taken from a CTFM 15-kHz–30-kHz sonar especially designed as a synthetic aperture sonar.

Keywords—Synthetic aperture(s) and underwater sonar, SAS.

I. INTRODUCTION

A SYNTHETIC aperture sonar, like any other active sonar, has to contend with the slow speed of sound propagation and the detection of echo signals in the presence of noise, reverberation, and multipath fading.

High-resolution imagery requires the use of signals of wide bandwidth. Coherent processing of wide bandwidth signals has also been shown to be advantageous for the reliable echo detection in the presence of noise, reverberation, and multipath. This is especially important since the slow speed of acoustic sound propagation means that transmitted pulse repetition rates are necessarily low, and, hence, the effective detection of every echo is required. In contrast, synthetic aperture radar, by virtue of its larger pulse repetition rate, can integrate many more echoes over the synthetic aperture and thus the signal-to-noise or reverberation (clutter) of each echo is not so critical.

The requirement for wide bandwidth signals, coupled with the fact that both medium and platform induced phase errors as well as absorption losses are proportional to frequency, means that signals for high-resolution synthetic aperture sonar applications are necessarily broad-band (i.e., signals with a large bandwidth-to-carrier frequency). In addition, broad-band signals can be employed to increase the pulse repetition rate, and hence the mapping rate, although at the expense of degraded image quality.

II. BROAD-BAND SIGNALS

There are a great number of waveforms suitable for echo

location. Each has unique characteristics that may be exploited to advantage in particular situations. While there have been a number of comparisons published on the various merits of different sonar signals it must be remembered that all sonars are constrained by the sonar equation, and that sufficient energy must be transmitted to allow for signal detection in the presence of noise. In many cases the performance of a particular waveform depends on the nature of the noise or reverberation environment. For example, as far as signal-to-white Gaussian noise is concerned, the choice of signal waveform and bandwidth is entirely arbitrary. However, for the case of a signal buried in impulsive noise, a long pulse of low power is superior to a short pulse of high power [1].

On the assumption that the processing is linear, a broad-band signal may be decomposed into a sequence or a number of narrow-band signals. As a consequence, broad-band signals may be generated using amplitude modulation (e.g., impulsive signals), frequency modulation (e.g., linear FM chirps, Costas arrays), phase modulation (e.g., BPSK), or a combination of modulation methods (e.g., pseudorandom noise). Sonars have been predominantly based on pulsed technology due to the simplicity of generating and processing of pulsed signals. However, to achieve broad-band operation using amplitude modulation requires narrow pulses, which are often subject to peak power limitations (e.g., cavitation) in an attempt to transmit sufficient signal energy for reliable echo detection. These impulsive signals enhance the nonlinear and dispersive properties of the medium—useful in certain seafloor imaging applications [2]—but because of their limited time-bandwidth product (approximately unity), no signal-to-noise or reverberation enhancement is possible by processing a single pulse. To lower the peak power level, it is necessary to increase the signal duration using pulse compression techniques (based on phase- and/or frequency-modulated spread spectrum techniques) to retain the signal bandwidth. These techniques are now commonplace with the advent of digital waveform synthesis and correlation methods.

Of the pulse compression techniques, the linear FM pulse (or chirp) is the most common example. An extreme case is continuous tone frequency modulation (CTFM), where the pulse length is equal to the pulse repetition period. This type of signal has a number of advantages for a synthetic aperture sonar relating to its continuous nature. The prime advantage of the CTFM signal is that it can provide continuous observation as the sonar traverses a target and hence any aspect dependent fluctuation is averaged. More importantly, phase

fluctuations due to varying path lengths may be averaged over the entire pulse repetition period. Furthermore, only very low peak power levels, well below the cavitation limit, are sufficient for reverberation limited operation. This suggests that CTFM is particularly suited to long-range high-frequency applications (i.e., where there are large absorption losses), where conventional sonars are noise limited because of peak power constraints. The advantage is lost in short-range low-frequency applications, however, where sonars tend to be reverberation limited. Finally, CTFM is a simple technique for generating a large bandwidth signal, but with a relatively slow change in instantaneous frequency (sweep rate). This slow linear frequency sweep simplifies the processing requirements considerably, since the broad-band CTFM signal can be readily divided into narrow-band components.

Unlike monostatic pulsed sonars, which only require one transducer time multiplexed between transmission and reception, separate transmit and receive transducers are required for continuous transmission sonars. Having separate transducers for transmission and reception means that the sonar is not "blind" for the duration of the transmitted pulse length, and are therefore useful for close range imaging. This is not usually a problem with side-scan synthetic aperture sonars where there is often a considerable distance to the nearest point of interest on the seafloor.

The major practical difficulty of continuous transmission sonars is the problem of coping with the very large dynamic range of received echo signals. The biggest signal is the direct acoustic crosstalk between the projector and hydrophone transducers. The smallest signal of interest is from a weak target at maximum range. With a pulsed sonar, acoustic crosstalk is avoided by gating off the receiver until the first desired echo is received. The dynamic range is further reduced using time varying gain (TVG) techniques. The equivalent processing for continuous signals is much more difficult to implement, and requires the use of swept notch filters in the case of CTFM or adaptive cancellation techniques to remove the unwanted crosstalk. To further reduce the acoustical crosstalk, the hydrophone should be isolated from the projector by as much as possible. This is not always feasible, in particular, when the sonar is mounted on a towfish. In this case, any direct acoustical coupling through the mounting system should be minimized, and acoustical baffles used to increase the acoustical path length between projector and hydrophone.

Broad-band acoustic transducers are comparatively easier to implement compared to their microwave counterparts for radar. The design of any wide bandwidth transducer is a continual trade-off between bandwidth and efficiency. An additional complication is introduced when the transducers are assembled arrays with mutual acoustic coupling altering performance. Using PZT discs as the active elements, we have designed and built 1-octave transducer arrays covering 15–30kHz at an efficiency of 60% [3]. Some high-frequency (1- to 2-MHz) transducers have been reported in the medical field; however, these designs appear to be of little value at seafloor mapping/imaging frequencies.

With broad-band signals there is a significant interaction between the signal waveform and beam pattern. For example, a narrowbeam CTFM sonar with an octave bandwidth, say, has a beamwidth that varies by a factor of two over the duration of the sweep. A number of methods have been proposed to ensure constant beamwidth operation with broadband signals [3], [4]. The simplest and most effective method is to use an array of transducers controlled by a frequency selective shading network. The idea is to control the effective aperture dimensions by shading the transducer array, so that the ratio of effective aperture size to wavelength is kept constant. However, the next section shows that it is not necessary or desirable for a synthetic aperture sonar to maintain a constant beamwidth with frequency in the horizontal direction (azimuth plane).

III. SYNTHETIC APERTURE SONAR

The theory of aperture synthesis has been well described in the literature, particularly with regard to synthetic aperture radar [5]–[10]. However, most of the theory has been largely developed in the context of narrow-band radar signals. This section briefly describes the salient features of synthetic aperture sonar and the ramifications of broad-band signals.

3.1. Resolution

The motivation for synthetic aperture side-scan processing is the property that the along-track resolution improves with the use of smaller transducers (antennas); the well-known result being that the nominal 3-dB resolution for focused processing is approximately half the horizontal dimension of the transducer ($L/2$). In practice, the nominal along-track resolution is slightly poorer than $L/2$ but the sidelobe level is lower. This is a result of a natural aperture shading imposed by the real beam pattern.

The fact that this along-track resolution is independent of range and wavelength is one of the desirable features of a synthetic aperture sonar. However, to achieve this result, it is necessary to synthesize a number of different length apertures, one for each focal range, and of a length corresponding to the width of the illumination on the seafloor at each focal range. Provided that the size of the synthetic aperture is varied for each received frequency component, the along-track resolution is independent of the transmitted bandwidth. Note that this assumes that the real beamwidth is wider for the lower frequency components and that the required aperture length to achieve the desired along-track resolution can be synthesized.

In practice, the along-track resolution is limited by the coherence of the medium and stability of the sonar. If the coherence length is shorter than the length of the desired synthetic aperture then there is a degradation in along-track resolution. Thus the resolution of targets at long ranges can be poorer than those at close ranges.

As with any narrowbeam sonar, the nominal cross-track resolution is determined by the bandwidth B of the echo signals and is of the order of $c/(2B)$, where c is the acoustic speed of propagation. This figure is degraded by medium

turbulence and dispersion and thus similarly degrades with range.

3.2. Mapping Rate

Aperture synthesis techniques are based on sampled apertures and thus the along-track spacing of the backscattered echo measurements must satisfy the sampling theorem. In theory, the along-track samples must be separated by no more than $\lambda_{min}/2$ on average; otherwise spatial aliasing will occur. In practice, the spatial frequencies are weighted by the two-way real beam pattern, and usually a controlled amount of aliasing is tolerated to allow wider sample spacing, and hence faster sonar speeds.

If the sample spacing is chosen to equal half the along-track length of an unshaded rectangular transducer, i.e., $\Delta L = L/2$, the grating lobes of the synthetic beam pattern (spatial frequency aliases) appear at the nulls of the real beam pattern, irrespective of the transmitted frequency, and are thus suppressed. However, if the samples are taken closer together, the grating lobes may coincide with the real beam pattern sidelobes and thus are not so well attenuated. To restrict the spatial frequency bandwidth, the two-way real beam pattern should ideally have a single mainlobe with negligible sidelobe structure in azimuth. For example, by shading the real aperture with a Dolph–Tchebychev weighting. This would limit the spatial frequency bandwidth to the extent of the angular width of the mainlobe and thus prevent the formation of grating lobes appearing outside the mainlobe of the real beam (provided $\Delta L \leq L/2$). Note that although the real beamwidth varies with frequency, the spatial bandwidth is kept constant at approximately $2/L$.

The primary differences between synthetic aperture radar and sonar arise due to many orders of magnitude difference in the respective propagation speeds. The information rate is lower for the sonar case and consequently the area mapping rate is lower. Undersampling the synthetic aperture can increase the mapping rate but this introduces angular image aliases as described above. Broad-band signals can help to smear these aliases into the image background [11], [12]. However, these ambiguous returns are a form of self-clutter and thus contribute to the background noise. Similarly, reducing the pulse repetition period introduces range ambiguities [13], [14]. Although an ambiguous target will be poorly imaged, due to the mismatch between its echo histories and that expected by the image reconstruction process, it will also introduce self-clutter.

In general, undersampling by a factor of N introduces N ambiguous image aliases, often each with an energy equivalent to the desired response [5]. Hence suppression of these ambiguous aliases increases the self-clutter N-fold, therefore, only those targets whose cross-section is sufficiently higher than the average cross-section per cell will be detectable. Thus with any of these under sampling schemes there is a trade-off between mapping rate and image quality.

The alternative method of increasing the mapping rate is to operate using N transducers. This improves the mapping rate by a factor of N, but at the expense of an increased hardware complexity [15]. Various configurations have been proposed,

for example, by having a multiplicity of transmitters either frequency or modulation coded [16]–[18], or multiple beams either horizontally [19] or vertically spaced [20]–[22]. The best approach for a broad-band system appears to be the use of a single wide transmitted beam with N adjacent widebeam hydrophone elements as a subarray [23], [24]. This method provides the most flexibility as the hydrophones may be coupled to act as one larger hydrophone, or as a number of smaller hydrophones, thus providing a variable along-track resolution capability without reducing the number of integrated echoes. In addition, the phase difference between pairs of hydrophones may be useful for determining the deviation of the sonar from a straight trajectory [25].

3.3. Signal-to-Noise Ratio

The derivation of the signal-to-noise ratio for a broad-band sonar is complicated by the frequency dependence of the various sonar parameters. For example, the echo level increases with frequency due to the increased projector directivity, but at the same time the absorption losses increase. At high frequencies, absorption losses dominate spreading losses, thus necessitating the use of low frequencies for long range imaging. The ambient sea-state noise is also frequency dependent, decreasing with frequency by approximately 5 dB per octave, but once again, at longer ranges the signal-to-noise ratio is dominated by the absorption losses at high frequencies [26]. Similarly, the target strength may vary with frequency, especially if the target has a plane surface. In this case the back-scattering is proportional to frequency and is also strongly aspect dependent.

It must be remembered that the traditional sonar equation is a narrow-band approximation. Therefore, derivation of the signal-to-noise ratio for a broad-band system requires computer modeling, taking into account any frequency dependence. In any case, unless the sonar is peak power limited, the output power is usually increased so that the sonar becomes reverberation, rather than sea noise, limited.

3.4. Reverberation

One of the advantages of a broad-band sonar is that any frequency-dependent target fluctuations are averaged. Similarly, any aspect dependent fluctuations are averaged by a widebeam sonar. This is an advantage of a synthetic aperture processing where we can transmit a widebeam and yet achieve a high along-track resolution. In addition, by transmitting a wide angle beam, the chance of picking up a strong specular echo returned at an oblique angle of incidence is increased. However, the disadvantage of transmitting a widebeam is that the reverberation signal increases.

In a synthetic aperture sonar the seafloor reverberation is unavoidable—this is the background against which targets are being imaged. The only way it can be reduced is by finer range gating, i.e., by having a shorter compressed pulse length, which implies a larger transmitted bandwidth. This also helps to reduce sea-surface reverberation and volume reverberation. Flying the sonar close to the seafloor to reduce the grazing angle may also reduce the seafloor reverberation but often the target strength as well.

Ideally, the transducer elevation beam pattern should be tailored to insonify only the swath of interest. This can be achieved by tilting the transducer to reduce seasurface reverberation and by maintaining a fixed elevation beam pattern with frequency. (However if an along-track resolution independent of frequency is required, the azimuth beam pattern should be frequency dependent.)

After synthetic aperture processing, the signal-to-reverberation ratio is improved because of the pulse integration along the synthetic aperture. The pulse integration improvement factor depends on the method of integration (i.e., whether coherent processing is used over the full synthetic aperture or if it is broken into smaller subapertures for multilook processing) and the statistics of the signal fluctuations. Assuming the somewhat artificial conditions of constant echo signal (i.e., no fading) and coherent processing over the full synthetic aperture, the pulse integration gives an improvement of $10 \log_{10} N$ in the signal to reverberation ratio. Here N is the effective number of integrated pulses (hits on target). This is proportional to length of the aperture synthesized L_s, and as this is dependent on the width of the real beam pattern, N varies with frequency as well as the range R.

$$N = \frac{L_s(\lambda, R)}{\Delta L} = \frac{\lambda R}{L \Delta L}. \qquad (1)$$

In practice, the target reflectivity is often to be aspect dependent, in particular specular targets, and thus the integration improvement factor is likely to be less than $10 \log_{10} N$.

Note that the use of a wider real beam spreads the transmitted energy over a wider area, but this is only partially compensated by the increased integration of the received signal in the case of volume reverberation [10] (spherical spreading losses are proportional to R^4 but the integration improvement factor is only proportional to R^2). However, after integration, the signal-to-surface reverberation ratio depends only upon the size of the resolution cell and is thus independent of the real beamwidth. Also note that sampling the aperture finer than $\Delta L/2$ will not further improve the signal-to-reverberation ratio unless, of course, the target strength fluctuates with sample position.

IV. IMAGE RECONSTRUCTION

The echo measured at sonar track position $y_i = i \Delta L$, assuming that there are J reflecting targets in a linear medium, can be represented by the convolution

$$e_i(t) = \sum_{j=1}^{J} s(t) \odot h(t, \tau_{ij}) \odot a_j(t, \theta_{ij})$$

$$\odot b_p(t, \theta_{ij}) \odot b_h(t, \theta_{ij}) \qquad (2)$$

where

$$\tau_{ij} = (2 R_{ij})/c \qquad (3)$$

$$\theta_{ij} = \sin^{-1} \frac{y_j - i \Delta L}{R_{ij}} \qquad (4)$$

$$R_{ij} = \left[(x_j)^2 + (y_j - i \Delta L)^2 \right]^{1/2} \qquad (5)$$

and where $s(t)$ is the transmitted signal, a_j is the impulse response of the jth target at a range of closest approach x_j, and along-track position y_j, b_p, and b_h are the impulse responses of the projector and hydrophone, and $h(t, \tau_{ij})$ is the impulse response of the medium. Equation (2) assumes that the projector and hydrophone are collocated and, for simplicity at this stage, that Doppler is ignored, i.e., the sonar moves to position $y_i = i \Delta L$ and makes a measurement, then moves to position y_{i+1} and makes the next measurement and so on. In the frequency domain, (2) may be transformed to yield

$$E_i(f) = \sum_{j=1}^{J} S(f) H(f, \tau_{ij}) A_j(f, \theta_{ij})$$

$$\cdot B_p(f, \theta_{ij}) B_h(f, \theta_{ij}) \qquad (6)$$

where a capital letter denotes the Fourier transform of the equivalent lower case quantity in (2).

4.1. Coherent Processing

To fully exploit the high-resolution capability of synthetic aperture systems, it is necessary to employ coherent focused processing. For broad-band signals this takes the form of a delay and sum beamformer where the echo signals along each synthetic aperture are time shifted to bring them into alignment at the desired focal range. These shifted echoes may then be summed to form the image at the focal point. (In comparison, unfocused operation directly sums the echoes without time delay compensation.)

It is also necessary to match-filter the echoes by weighting them in proportion to their expected signal-to-noise ratio, effectively placing less emphasis on the data of poorer quality. For example, the echoes from on-axis targets are likely to be stronger than those off-axis due to the response of the sonar beam patterns. Ideally, we would like to deconvolve the transmitted signal, medium, and transducer responses from the echo signal, but in the presence of noise (assumed additive, white Gaussian noise) the matched filter is the optimal processor. In practice, the form of this filter would depend on the power spectral density of the reverberation signal [27], but this is assumed flat for the present discussion.

For the synthetic aperture centered on the sonar position y_i, the delay and sum beamforming operation may thus be represented as

$$c_i(t) = \sum_{k=k_{min}}^{k_{max}} \left\{ \sum_{n=-N/2}^{(N-1)/2} e_{i+n}(t) \star s(t) \right.$$

$$\left. \odot \delta(t + \Delta \tau_{nk}) \star b(t, \theta_{nk}) \right\} \text{rect} \left(\frac{t - \tau_k}{\Delta \tau} \right) \qquad (7)$$

or equivalently in the frequency domain as

$$C_i(f) = \sum_{k=k_{min}}^{k_{max}} \left\{ \sum_{n=-N/2}^{(N-1)/2} E_{i+n}(f) S^*(f) \right.$$

$$\left. \cdot e^{j2\pi f \Delta \tau_{nk}} B^*(f, \theta_{nk}) \right\} \odot \Delta \tau \, \text{sinc} \, (f \Delta \tau) e^{-j2\pi f \tau_k} \qquad (8)$$

where $\star$ denotes correlation, $b(t, \theta_{nk}) = b_p(t, \theta_{nk}) \odot b_h(t, \theta_{nk})$ is the combined two-way beam pattern impulse response, and where

$$\tau_k = (2k \Delta R)/c \qquad (9)$$

$$\Delta \tau = (2 \Delta R)/c \qquad (10)$$

$$\tau_{nk} = (2R_{nk})/c \qquad (11)$$

$$\Delta \tau_{nk} = \tau_{nk} - \tau_k \qquad (12)$$

$$R_{nk} = \left[(k \Delta R)^2 + (n \Delta L)^2 \right]^{1/2} \qquad (13)$$

$$\theta_{nk} = \tan^{-1} \frac{n \Delta L}{k \Delta R} \qquad (14)$$

$$N \approx \left[\frac{ck \Delta R}{fL \Delta L} \right]. \qquad (15)$$

R_{nk} and θ_{nk} are the range and angle in azimuth to the kth focal range ($R_k = k \Delta R$) from the nth echo measurement (relative to the track position i being reconstructed), $\Delta \tau_{nk}$ is the required time correction, $\Delta \tau$ is the width of the range gates, and N is an integer specifying how many echo measurements to integrate along the length of the synthetic aperture ($L_s = N \Delta L$).

With reference to (8), the image reconstruction process may be viewed as a two-stage matched filtering/correlation process. Firstly, the echo signals are compressed in range by multiplication with $S^*(f)$, the range compression matched filter response. The echoes are then weighted in azimuth by $B^*(f, \theta_{nk})$, phase shifted by $\exp(j2\pi f \Delta \tau_{nk})$ to align the echoes at the desired focal range, and then coherently summed over the length of the synthetic aperture. (This effectively is a matched filtering process to compress the azimuth beamwidth of the synthetic aperture.) Finally, the out-of-focus ranges are rejected by the range gating function $\text{rect}((t - \tau_k)/\Delta \tau)$.

Note that a number of focal ranges are required to span the width of the imaging region (from $R_{\min} = k_{\min} \Delta R$ to $R_{\max} = k_{\max} \Delta R$). The width of the range gates can be determined from consideration of the depth of field at the focal range R_f. This is approximately $4\lambda(R_f/L_s)^2$, where R_f/L_s is the f-number of the synthetic aperture of length L_s. For a constant along-track resolution independent of focal range, the f-number is kept constant at L/λ, thus giving a depth of field of $4L^2/\lambda$. Therefore, the greater the desired along-track resolution $L/2$, the shorter the depth of field, and thus the greater the required computation.

Where Doppler effects are minimal, such as with low-speed and/or narrowbeam side-scan sonars, the term $S^*(f)$ in (8) may be moved outside the inner summation over n. In this case the image reconstruction process may be split into a range matched filter/correlator followed by an azimuth matched filter/correlator. The range matched filter is usually performed in real-time as the data is being received followed by the azimuth compression (beamforming) of selected regions of interest (usually performed off-line due to the computation requirements).

In practice, the echo signals are time sampled and it is not easy to shift the sampled echo signals by the required time delays, as this often requires time delays that are fractions of the sampling period. Interpolation functions are required to delay the echo waveform by noninteger fractions of the sampling period. However, the equivalent process is often simpler in the frequency domain, where time delays are replaced by frequency-dependent phase shifts. Similarly, the correlations required in the time-domain transform into multiplications in the frequency domain.

While it is expedient to perform the delay and sum operations in the frequency domain, the range gating operation is easier to perform in the time domain. However, the full inverse Fourier transform need not be calculated for the frequency-domain algorithm since it is followed by the range gating operation. Thus (7) and (8) may be recast as

$$c_i(t) = \sum_{k=k_{\min}}^{k_{\max}} \left\{ \int_{-f_{\max}}^{f_{\max}} \sum_{n=-N/2}^{(N-1)/2} E_{i+n}(f) \cdot F_{nk}^*(f) e^{+j2\pi ft} \, df \right\} \text{rect} \left(\frac{t - \tau_k}{\Delta t} \right) \qquad (16)$$

where $W = f_{\max} - f_{\min}$ is the frequency extent of the sonar system and where

$$F_{nk}^*(f) = S^*(f) e^{j2\pi f \Delta \tau_{nk}} B^*(f, \theta_{nk}). \qquad (17)$$

The computation required for the image reconstruction may be reduced by noting that the summation over n in (16) is in fact a correlation of $E_i(f)$ with $F_{ik}(f)$. Thus transforming the appropriate quantities of (16) into the spatial frequency domain yields

$$c_i(t) = \sum_{k=k_{\min}}^{k_{\max}} \left\{ \int_{-f_{\max}}^{f_{\max}} \sum_{u=-N/2}^{(N-1)/2} \bar{E}_u(f) \bar{F}_{uk}^*(f) \cdot e^{j2\pi iu/N} e^{+j2\pi ft} \, df \right\} \text{rect} \left(\frac{t - \tau_k}{\Delta \tau} \right) \qquad (18)$$

where a bar over a quantity denotes a spatial discrete Fourier transform (DFT) of that quantity (in the i or along-track direction) and u is the spatial frequency, e.g.,

$$\bar{E}_u(f) = \sum_{i=-N/2}^{(N-1)/2} E_i(f) e^{-j2\pi iu/N}. \qquad (19)$$

Finally, after demodulation of $c_i(t)$ to baseband, the resultant image can be described as

$$\text{image}[i, q] = |\tilde{c}_i(q \Delta t)|^2 \qquad (20)$$

where $\tilde{c}_i(t)$ is the complex envelope of $c_i(t)$, and where the image pixels are spaced on a grid of ΔL by $c \Delta t/2$. Note that if the aperture has been spatially undersampled (say by having ΔL too large), the reconstruction algorithm must be modified so that image along-track sample spacing satisfies the sampling requirement. Even though the image will have artifacts (aliases) due to the undersampling, it is necessary to sample the image sufficiently to prevent missing image detail. The same argument applies for the spacing of the image

pixels in the cross-track direction. Here Δt needs to be smaller than the reciprocal of the transmitted bandwidth B.

There are several other aspects of this reconstruction process to note. Firstly, the medium is assumed to be time stationary, homogeneous, and nondispersive, i.e.,

$$H(f, \tau) = e^{-j2\pi f\tau} \qquad (21)$$

where spreading and absorption losses have been assumed to be compensated for in the sonar receiver. With the medium assumed to be homogeneous—i.e., a constant refractive index—signals travel with a constant speed of propagation, ray paths are straight, and the acoustic path length is simply twice the slant range. Refraction effects due to a varying speed of sound profile can be incorporated using ray tracing techniques. This enables the acoustic path lengths, and thus the required time-delay corrections $\Delta\tau_{nk}$, to be calculated, provided of course the sound speed profile is known [28].

Secondly, at some stage during the reconstruction process it is necessary to demodulate the bandpass signals to baseband. Usually it is computationally expedient to convert the bandpass echo signals into quadrature baseband components as soon as possible, since this allows the sampling rate of the subsequent processing to be lowered. If this is the case, then all the quantities in the preceding equations should be replaced with their complex quadrature baseband equivalents. For example, (7) becomes

$$\tilde{c}_i(t) = \tfrac{1}{8} \sum_{k=k_{min}}^{k_{max}} \left\{ \sum_{n=-N/2}^{(N-1)/2} \tilde{e}_{i+n}(t) \star \tilde{s}(t) \right.$$
$$\left. \odot \tilde{\delta}(t + \Delta\tau_{nk}) \star \tilde{b}(t, \theta_{nk}) \right\} \mathrm{rect}\left(\frac{t - \tau_k}{\Delta\tau}\right) \quad (22)$$

where $\tilde{s}(t) = s_+(t)\exp(-j2\pi f_c t)$ is the complex envelope, $s_+(t) = s(t) + j\hat{s}(t)$ is the pre-envelope, and $\hat{s}(t)$ is the Hilbert transform of $s(t)$. The other variables may be derived in a similar fashion. Equation (16) may now be rewritten in the complex notation as

$$\tilde{c}_i(t) = \tfrac{1}{8} \sum_{k=k_{min}}^{k_{max}} \left\{ \int_{-W/2}^{W/2} \sum_{n=-N/2}^{(N-1)/2} \tilde{E}_{i+n}(f)\tilde{F}_{nk}(f) \right.$$
$$\left. \cdot e^{+j2\pi ft} \, df \right\} \mathrm{rect}\left(\frac{t - \tau_k}{\Delta\tau}\right) \quad (23)$$

where the limits on the integral have been reduced from f_{max} to $W/2$ thus reducing the computation requirements, particularly if the system is narrow band.

It should be noted that even synthetic aperture radars using pulse compression techniques (e.g., chirped signals) are still very much narrow band, with $B/f_c < 0.1$ where f_c is the carrier or center frequency of the band. This leads to simplifications in the image reconstruction since any frequency dependence may be neglected. Thus (6) reduces to

$$E_i(f) = \sum_{j=1}^{J} S(f)H(f, \tau_{ij})a_j(\theta_{ij})b_p(\theta_{ij})b_h(\theta_{ij}). \quad (24)$$

More importantly, the time shifts required to align the echoes

in the focusing process simplify to a frequency-independent phase shift operation that can be performed in the time domain. Similarly, the beam pattern correlation reduces to a simple weighting operation. With these modifications the reconstruction algorithm described by (22) now simplifies to

$$\tilde{c}_i(t) = \tfrac{1}{2} \sum_{k=k_{min}}^{k_{max}} \left\{ \sum_{n=-N/2}^{(N-1)/2} \left(\tilde{e}_{i+n}(t) \star \tilde{s}(t)\right) \right.$$
$$\left. \cdot e^{j2\pi f_c \Delta\tau_{nk}} b(\theta_{nk}) \right\} \mathrm{rect}\left(\frac{t - \tau_k}{\Delta\tau}\right). \quad (25)$$

This is the standard narrow-band reconstruction algorithm where range curvature is negligible, for example in narrow beam applications. In addition, the hyperbolic phase shift required to focus the aperture $\Delta\tau_{nk}$ may be approximated to a quadratic function of n. This has an important computational advantage when the along-track correlation operation is transformed into the spatial frequency domain, similar to (18), since the inverse DFT operation can be avoided using step transform type methods [29], [30].

An alternative method of broad-band synthetic aperture reconstruction is to filter the broad-band echoes into an ensemble of narrow-band components. These can then be individually processed (in parallel if need be) using narrow-band synthetic aperture reconstruction techniques, such as those employed with synthetic aperture radar data. The ensemble of reconstructed narrow-band images are then combined to form the resultant image. This technique is termed spectral decomposition because many narrow-band signals are derived from a single broad-band signal, and has been used with both impulsive signals [31] and linear FM sweeps [11]. It is also desirable, if possible, to split long duration signals into shorter components for processing. This is because any sonar/target motion has a greater effect on longer duration signals [5]. The processing of these shorter length components is often less complicated than processing the entire signal, and afterwards they can be recombined to produce the desired resolution.

4.2. Noncoherent Processing

Noncoherent or envelope processing is a technique proposed to allow aperture synthesis when the echo signals lack phase coherence [32]. It is a suboptimal method (in the sense that the potential resolution is poorer) but has the advantage that the sonar position need only be known to within a fraction of the (effective) pulse length, rather than the carrier wavelength [33], [34]. Envelope processing is therefore quite robust. Instead of using the echo phase, envelope processing is based on the range curvature effect. An image point is reconstructed by summing the intensities of the measured data along the expected range curvature locus, or by radially back-projecting the intensity of the measured data [35]. Like back-projection techniques used in computed tomography, envelope processing produces a bright point at the target position sitting on a background "fog." Obviously, the finer the range resolution and the wider the beamwidth, the greater the signal-to-background ratio.

The image reconstructed using focused envelope processing may be described by

$$\text{image}_{\text{env}}[i, q] = p_i(q\,\Delta t) \tag{26}$$

where

$$p_i(t) = \tfrac{1}{2} \sum_{k=k_{\min}}^{k_{\max}} \sum_{n=-N/2}^{(N-1)/2} \left| \int_{-W/2}^{W/2} \tilde{E}_{i+n}(f) \right.$$
$$\left. \cdot \tilde{F}_{nk}^*(f) e^{+j2\pi f t}\, df \right|^2 \text{rect}\left(\frac{t - \tau_k}{\Delta \tau}\right). \tag{27}$$

Like coherent processing, envelope processing may be unfocused to reduce the computation required by setting $\Delta\tau_{nk} = 0$ in (17).

Strictly speaking, noncoherent integration does not improve the signal-to-noise ratio of the image. However, for fluctuating targets and background, it is well known that noncoherent integration of N pulses produces an improvement of detection equivalent to approximately $5\log_{10} N$, instead of $10\log_{10} N$ achievable with coherent integration. This improvement is due to the fluctuations in the target and background being averaged, rather than a cancellation of the noise. With these envelope processing schemes "robustness" is obtained at the cost of reduced resolution and signal-to-background ratio [32]. However, summation on an intensity basis results in a significant reduction in speckle, leading to an enhancement in the image contrast.

4.3. CTFM Processing

The reconstruction techniques presented in this paper have been for arbitrary broad-band signals. Often the reconstruction process may be simplified by exploiting certain features of specific signals as will be shown in this section from a consideration of CTFM signals. The most common CTFM signal is based on a linear FM pulse of the form

$$s_i(t) = \text{rect}\left(\frac{t - \tfrac{1}{2}T}{T}\right) \cos\left[2\pi\left(f_0 t + \tfrac{1}{2}\mu t^2\right)\right] \tag{28}$$

where f_0 is the initial frequency, μ is the sweep rate, and T is the sweep period, giving a bandwidth of approximately μT. Repeating this linear FM pulse every T seconds forms a continuous signal (albeit with a frequency discontinuity at $t = iT$). This can be expressed in terms of a convolution of a single pulse with a replicating function, i.e.,

$$s(t) = \sum_i s_i(t - iT) = s_i(t) \odot \sum_i \delta(t - iT). \tag{29}$$

To range match-filter this CTFM signal we ideally would like to correlate the echo signals with a replica of the transmitted signal, i.e.,

$$g_i(t) = e_i(t) \star s_i(t). \tag{30}$$

In the past this has been a formidable operation for broad-band continuous signals due to the size of the correlation. Even demodulation of the signals to baseband presents only a small computational saving. Besides, this requires the use of a pair of filters, accurately phase matched over the bandwidth of the

signal. Although this is a simple digital signal processing operation, it is difficult to implement using analog filters. Consequently, other techniques have been applied to reduce the computation.

The traditional method using analog electronics exploits the frequency relationship between the echo and transmitted signals by demodulating the echo signals by the transmitted signal. This produces constant difference frequencies that are proportional to the target delays. There is, however, a problem of distinguishing between echoes emanating from the current sweep with those from the previous sweep. One technique to overcome this ambiguity is called dual-demodulation where two reference sweeps are employed [36]. The output of a CTFM dual-demodulator, for a single echo of amplitude A (ignoring any frequency dependence) delayed by τ, can be described by

$$d_i(t, \tau) = A\cos\left[2\pi\mu\tau t + 2\pi f_0\tau - \pi\mu\tau^2\right] \tag{31}$$

$$= A\cos\left[2\pi\mu\tau(t - t_p)\right] \quad \tau \le t - iT < T + \tau \tag{32}$$

where $t_p = \tau/2 - f_0/\mu$. This signal represents a constant frequency $\mu\tau$ proportional to the echo delay τ with a phase discontinuity at $t = iT + \tau$, unless the demodulated frequency $\mu\tau$ is a multiple of the prf, $1/T$.

The final part of the matched filtering operation is to calculate the Fourier transform of the demodulated signals, usually by means of a FFT operation. In order to achieve the full resolution capability of the CTFM signal it is necessary to use an FFT that spans an entire sweep period T. However, since the echo signals are staggered in time, no single block FFT can produce valid output data for all ranges. To overcome this problem, overlapping FFT's can be used, but this significantly reduces the computational efficiency since most of the data from each FFT must be discarded. Alternatively, the output resolution may be sacrificed by taking shorter length FFT's. Each shorter FFT contains fewer invalid data points, and therefore, less overlap is required. Moreover, these shorter length FFT's may be reordered and combined to form a number of longer overlapping FFT's. The resolution is now the same as before, but since the FFT's are shorter and less overlap is required, the computation requirements are reduced. Refer also to a similar SAR azimuth matched filtering technique called the step transform [29], [30].

Following the approach of using shorter length FFT's, the demodulated signal may be split into M frames per sweep, each of duration $T_m = T/M$, where the mth frame of the ith sweep is given by

$$d_{im}(t, \tau) = A\,\text{rect}\left(\frac{t - t_m}{T_m}\right) \cos\left[2\pi\mu\tau(t - t_p)\right]$$
$$\cdot \tau \le t - iT < T + \tau \tag{33}$$

where $t_m = (m + 0.5)T_m$ is the time center of the mth frame relative to the start of the last transmitted sweep.

The desired range match-filtered signal, $\tilde{g}_{im}(t)$, may be

derived from the demodulated signal $d_{im}(t)$ by calculating

$$\tilde{g}_{im}(t) = 2D_{im}(\mu t)U(\mu t) \tag{34}$$

where $U(t)$ is the unit step function to suppress the negative delay components and where $D_{im}(\nu)$ is the Fourier transform of $d_{im}(t)$, evaluated at $\nu = \mu\tau$, i.e.,

$$D_{im}(\nu, \tau) = \frac{1}{2}AT_m \text{ sinc }(\nu T_m)e^{-j2\pi\nu t_m}$$

$$\odot \left[\delta(\nu + \mu\tau) + \delta(\nu - \mu\tau)\right]e^{-j2\pi\nu t_p}. \tag{35}$$

Note that although there may be some interference between the overlapping sidelobes of the sinc functions centered at $\nu = \pm\mu\tau$ for close range targets, this is often of little concern. The sidelobes may be reduced by applying a window function before the FFT operation. However, the frames must now be overlapped to prevent loss of information.

The coherent focused reconstruction algorithm described by (22) may be modified to yield

$$\tilde{c}_{im}(t) = \frac{1}{2}\sum_{k=k_{min}}^{k_{max}} \left\{ \sum_{n=-N/2}^{N/2} \left(\tilde{g}_{i+n,m}(t) \odot \tilde{\delta}(t + \Delta\tau_{nk})\right) \right.$$

$$\left. \cdot B(f_m, \theta_{nk})e^{-j2\pi(f_0+\mu(t'_m-\tau_{nk}/2)\tau_{nk})} \right\}$$

$$\cdot \text{ rect}\left(\frac{t - \tau_k}{\Delta\tau}\right) \tag{36}$$

where

$$f_m = f_0 + \mu(t'_m - \tau_{nk}) \tag{37}$$

is the mean received frequency of the mth frame for the echoes delayed by τ_{nk}, and where

$$t'_m = \begin{cases} t_m & t_m \geq \tau_{nk} \\ t_m + T & t_m < \tau_{nk} \end{cases}. \tag{38}$$

The convolution operation in (36) corrects for range curvature and the phase-correction term removes the delay-dependent phase shifts resulting from the demodulation process. The term $f_0 + \mu(t'_m - \tau_{nk}/2)$ is the average of the received and extrapolated transmitted frequency (the frequency that would have been transmitted if the sweep was not reset, but allowed to continue) at time t'_m. The algorithm assumes that the number of frames M is large enough so that narrow-band approximations are valid in the reconstruction process. For example, the beam pattern responses may be considered constant (at each reconstruction frequency) and thus only a simple weighting is necessary.

The ensemble of M narrow-band images generated using (36) may be combined in a number of different ways. The simplest method is to simply add the intensities of each of the narrow-band images, i.e.,

$$\text{image}_{nc}[i, q] = \sum_{m=1}^{M} |\tilde{c}_{im}(q\Delta t')|^2 \tag{39}$$

where $\text{image}_{nc}[i, q]$ is the image resulting from the noncoherent addition. Here $\Delta t'$ needs to be smaller than the delay resolution obtained using the reduced bandwidth B/M.

Aside from its simplicity, noncoherent addition is robust with regard to the effects of frequency-dependent phase errors introduced by the medium and any analog filters in the receiver electronics. Moreover, noncoherent addition has the important advantage that it may reduce the coherent speckle found in each of the narrow-band images.

Alternatively, the ensemble of narrow-band complex images may be coherently added together to produce a high-resolution coherent image, where

$$\text{image}_{co}[i, q] = \left| \sum_{m=1}^{M} \tilde{c}_{im}(q\Delta t) \right|^2. \tag{40}$$

Note that it is necessary to compute the narrow-band images using a finer pixel grid in cross-track, commensurate with the increased range resolution obtained using the full transmitted bandwidth $B \approx \mu T$.

4.4. Doppler Considerations

The stop-and-go scenario used in this paper is a simplification and in practice the sonar moves continuously along its track as it transmits pulses and receives the echoes. This has two major effects that must be considered, especially when fast platform speeds and long propagation delays are expected.

Firstly, the moving sonar subjects the transmitted pulse and received echo signals to the Doppler effect. The Doppler effect distorts the echo signals and thus corrections are required to avoid decorrelations in the image reconstruction process. Secondly, since the sonar moves during the propagation of the pulses, the echoes from any one transmitted pulse are received at different places along the aperture depending on the echo delay. Thus the resultant image is skewed slightly in the along-track direction, with the skew proportional to the sonar along-track speed.

The modifications required to the reconstruction process to accommodate Doppler distortions may be determined from consideration of the Doppler distorted echo spectrum. Incorporating the signal time compression due to Doppler, (6) becomes

$$E_i(f) = \sum_{j=1}^{J} \frac{1}{\sqrt{\eta_{ij}}} S(f/\eta_{ij})H(f/\eta'_{ij}, \tau_{ij})A_j(f/\eta'_{ij}, \theta_{ij})$$

$$\cdot B_p(f/\eta_{ij}, \theta_{ij})B_h(f/\eta'_{ij}, \theta_{ij}) \tag{41}$$

where the frequency scaling (time compression) factors are given by

$$\eta'_{ij} = 1 + a\sin\theta_{ij} \tag{42}$$

$$\eta_{ij} = \frac{1 + a\sin\theta_{ij}}{1 - a\sin\theta_{ij}} \approx 2\eta'_{ij} \tag{43}$$

for $a = v/c$ where v is the along-track sonar speed. As a comparison, a narrow-band approximation to (41) is

$$E_i(f) = \sum_{j=1}^{J} S(f - \Delta f_{ij})H(f, \tau_{ij})a_j(\theta_{ij})b_p(\theta_{ij})b_h(\theta_{ij})$$

$$\tag{44}$$

where $\Delta f_{ij} = f_c(\eta_{ij} - 1) \approx 2v \sin \theta / \lambda$ is the Doppler shift of the carrier frequency.

Here we have assumed a stationary medium and stationary targets and that the range rate ($v \sin \theta$) is constant over the pulse duration (so that the higher order range derivatives are zero). The amplitude scale factor represents the change in echo amplitude due to the Doppler time compression, but is negligible and may be ignored. Note that on projection into the water, the transmitted frequencies are Doppler shifted and similarly on reception the reflected echo frequencies are again Doppler shifted. In comparison, radar Doppler only depends on the relative radar/target motion. However, for the assumed case of a stationary target in a stationary medium, the sonar Doppler is equivalent to radar Doppler apart from a different amplitude scale factor due to the quantum nature of electromagnetic waves.

From inspection of (41) it may be seen that the Doppler distortion depends upon the sonar speed and the target angle and as a consequence of the latter, the pulse compression operation cannot be performed independently of the azimuth compression operation. The received echoes must now be correlated with different Doppler distorted replicas of the transmitted signal, depending on the target angle from boresight. In practice, the Doppler distortions at typical two speeds are small, especially with narrow-beam operation. In fact, the strongest echo reflections with a side-scan sonar are usually on axis and thus are subject to little or no Doppler. The correction becomes more important for spotlight mode operation or if the sonar beams are scanned ahead of broadside.

One might think that since the Doppler shift depends on the target angle from the sonar, this additional information may be used to indicate more precisely where a target is, even if it just indicates that the target is fore or aft of the sonar by the up or down Doppler shift. However, while this Doppler shift does improve the instantaneous angular resolution of the sonar, the trade-off is that there is now an increased range ambiguity, regardless of the form of the transmitted signal [5]. This trade-off is usually illustrated by means of the ambiguity function/diagram for the signal under consideration. It is important to note that the resolving power of a synthetic aperture sonar is dependent upon the system geometry regardless of the effects of Doppler.

To determine the image skew, the propagation delay $\tau(y)$ can be written as a function of the instantaneous sonar position $y = vt$ as

$$\tau(y) = \frac{2R(y)(c + v \sin \theta(y))}{c(1 - a^2)}$$

$$= \frac{2R(y)}{c(1 - a^2)} + \frac{2v(y_t - y)}{c(1 - a^2)} \qquad (45)$$

where $R(y), \theta(y)$ are the target range and azimuth angle at the instant of reception, y_t is along-track target position, and $a = v/c$. Note that the sonar has moved a distance $v\tau(y)$ along the aperture during the signal propagation time. If necessary, the first term in (45) can be compensated by scaling the wavelengths used in the reconstruction by $(1 -$

a^2). However, this correction is usually extremely small and can be neglected. The second term represents an additional Doppler shift of $2va/(1 - a^2)\lambda$ [37]. This is a constant term and produces the slight skew of the image in azimuth. The skew can be compensated by inserting a linear phase taper (at each frequency) across the receiving synthetic aperture, so that the synthetic beam is steered forward by an angle of $2a/(1 - a^2)$ (cf., [14]).

V. COMPARISON OF SIMULATION AND EXPERIMENTAL RESULTS

To illustrate aspects of the reconstruction process, images reconstructed from both real data and computer simulated data are now presented. The real data was obtained from a wire guided synthetic aperture experiment performed in Loch Linnhe, Scotland, where a large steel buoy was anchored to the seafloor using concrete blocks to act as a known test target. For the experimental details refer to [11], and for the sonar parameters see Table I. Experimental considerations meant that the slowest speed that the sonar could be moved along the cableway was approximately 1 knot. With the transducer dimensions employed, this meant that the aperture was undersampled by a factor of about three times the desired minimum value. Regardless of the aperture undersampling, it was felt that it was better to traverse the synthetic aperture quickly to reduce the effects of both towfish wander and medium turbulence.

The computer simulation used a simple model of a CTFM side-scan sonar in an ideal medium, based on (2) modified for Doppler effects. Despite its simplicity, the computer simulation was found to be essential for verification of the reconstruction algorithms. For purposes of comparison with the real measured data, an idealized "point" target was modeled in approximately the same position as the real target with all other parameters being equal.

Note that all images are normalized intensity distributions plotted on a linear scale and show only a small portion of the available swath. The sonar track is off the lower left-hand edge of each image and proceeds from right to left, and the nearest displayed range is 65 m from the track, except in the expanded resolution images which are centered on the test target. All the synthetic aperture reconstructions were performed over the width of the real beam mainlobe, i.e., null-to-null.

The intensity distribution of the measured data is shown in Fig. 1 for (a) frame 8 and (b) frame 15. For the range swath presented, frame 8 roughly corresponds to a mean received frequency of 26 kHz whereas frame 8 corresponds to 21 kHz. Although the along-track resolution is predictably poor because of the widebeam operation, at least two targets at different ranges are apparent for frame 15. The closer target (66.5 m) is the desired test-target, but the identity of the other target is unknown. This could be a reflection from the floating marker buoy (and coil of unused rope) used to mark the presence of the test target. This mysterious target appears to lie almost normal to the end of the cableway, and is therefore only detected at the low end of the frequency sweep when the beamwidths are wider (hence it is not so noticeable

TABLE I
SUMMARY OF OPERATING PARAMETERS FOR THE PROTOTYPE
CTFM SYNTHETIC APERTURE SONAR

Hydrophone length	$L = 255$ mm
Hydrophone width	$D_h = 65$ mm
Projector length	$L_p = 223$ mm
Projector width	$D_p = 55$ mm
Initial transmitted frequency	$f_0 = 30.0$ kHz
Terminal transmitted frequency	$f_1 = 15.0$ kHz
Sweep period	$T = 0.8192$ s
Sweep rate	$\mu = -18.3105$ kHz/s
Number of frames per sweep	$M = 20$
Frame duration	$T_m = 40.96$ ms
Frame bandwidth	$B_m = 750$ Hz
Towfish speed	$v = 0.51$ m s^{-1}

for frame 8), and when the sonar is near the end of the cableway. The along-track resolution of frame 15 is noticeably poorer than frame 8 because of the wider beamwidth at the lower frequency.

With the computer simulation, any frequency or aspect dependence of the simulated target strength was ignored, i.e., $a(t, \theta) = a\delta(t)$. By comparison, the measured data certainly fluctuates noticeably with aspect and frequency. However, after application of coherent, focused, synthetic aperture processing (refer to Figs. 2 and 3) the real and simulated image reconstructions are quite similar. The measured data has a slightly poorer range resolution than that of the simulated data. This is probably due to dispersion effects of the medium and receiver electronics, and possibly due to multipath effects (the surface reflected path is approximately 0.5 m longer than the direct path). It should also be noted that both the measured and simulated data had a Hamming window applied to reduce the range sidelobe level.

Although the along-track resolution should be independent of frequency (compare Figs. 2(d) and 3(d)) the real reconstructed image reconstructed for frame 8 (Fig. 2(c)) has more sidelobe structure than the image reconstructed for frame 15 (Fig. 3(c)). This is probably due to any path length fluctuations producing greater phase errors at the higher frequencies. By comparison with the measured data, the sidelobe structure of the simulated reconstruction is minimal. This is a consequence of the aperture shading resulting from the real beam patterns, and of course, the absence of any phase errors.

From inspection of Figs. 2 and 3 it is apparent from the presence of the ambiguous target aliases that the aperture has been spatially undersampled. Note how the positions of these aliases vary with frequency. After addition of all 20 narrow-band images these aliases are smeared into the background. This is more effective if the narrow-band images are coherently combined using (40) (as illustrated in Fig. 4(c) and (d)) rather than when they are noncoherently combined using (39) (Fig. 4(a) and (b)). It is also interesting to note that the resolution obtained with the measured data is comparable with the simulated reconstruction and with theory. Using a transmitted bandwidth of 30 kHz, the theoretical cross-track resolution is of the order of 5 cm and with a transducer dimension of approximately 25 cm the expected along-track resolution is 12.5 cm.

(a)

(b)

(c)

(d)
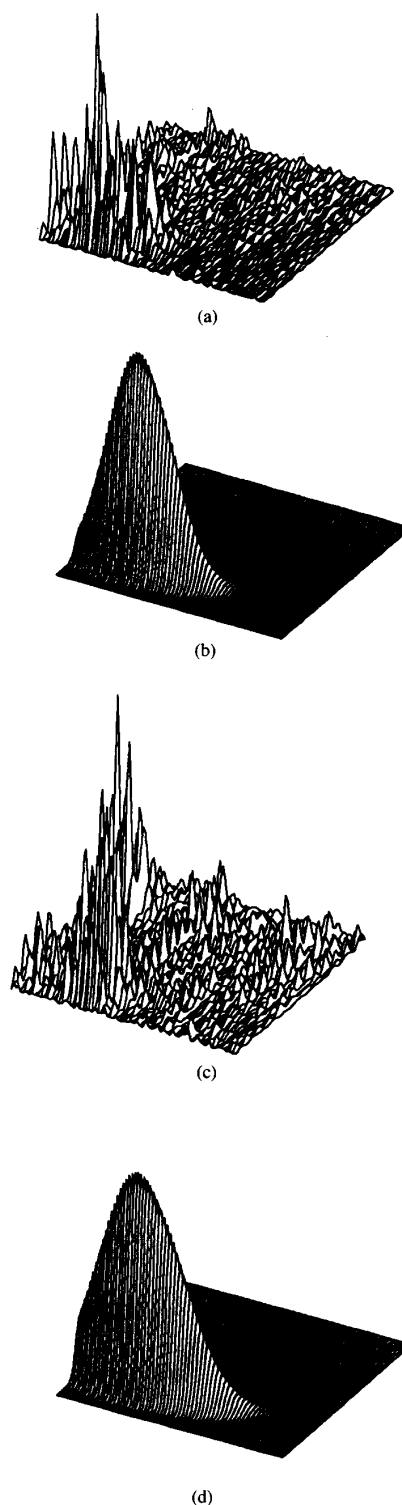
Fig. 1. The intensity distribution of the range-gated data for (a) the real target (frame 8), (b) the simulated target (frame 8), (c) the real target (frame 15), and (d) the simulated target (frame 15). Note that for the range swath shown, frame 8 corresponds to 26 kHz and frame 15 corresponds to 21 kHz. The along-track dimension is 32 m and the range swath covers 16 m offset by 65 m from the sonar track.

(a)

(b)

(c)

(d)
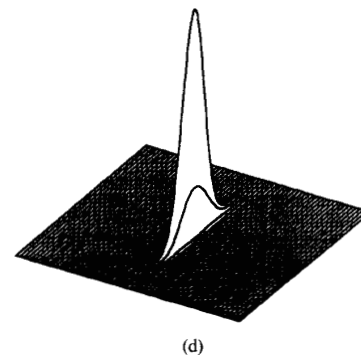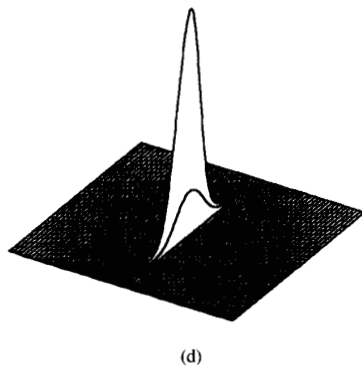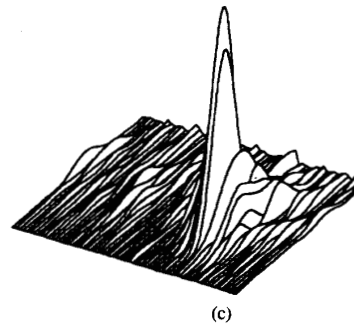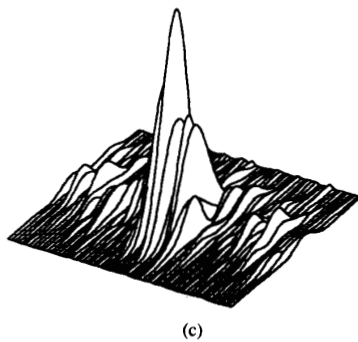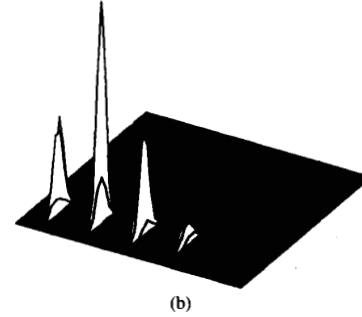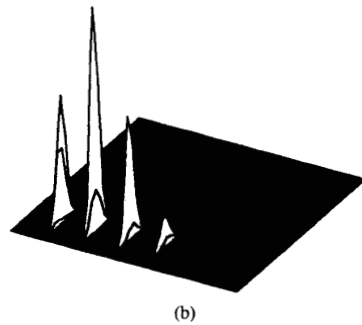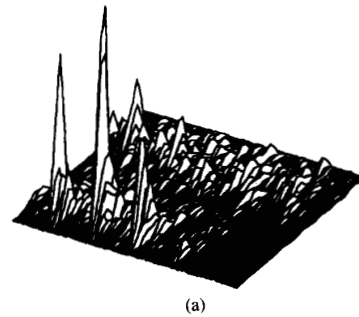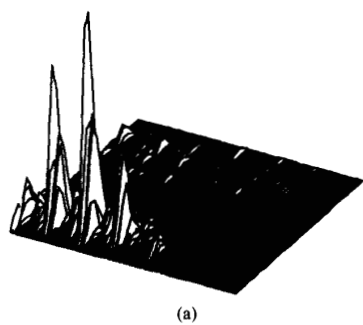
Fig. 2.   The intensity distribution of a narrow-band image of the test target reconstructed using frame 8 ($\approx$ 26 kHz for the cross-track swath shown) for (a) the real data, (b) the simulated data. The image distributions are calculated on a pixel grid of 0.5 m cross-track by 0.1 m along-track, and cover a total area of 16 m by 32 m. The image distributions of (c) and (d) are expanded versions of (a) and (b) centered on the target, and calculated on a pixel grid of 0.05 m cross-track by 0.1 m along-track, covering an area of 6.4 m by 6.4 m.

(a)

(b)

(c)

(d)

Fig. 3.   The intensity distribution of a narrow-band image of the test target reconstructed using frame 15 ($\approx$ 21 kHz for the cross-track swath shown) for (a) the real data, and (b) the simulated data. The image distributions are calculated on a pixel grid of 0.5 m cross-track by 0.1 m along-track, and cover a total area of 16 m by 32 m. The image distributions of (c) and (d) are expanded versions of (a) and (b) centered on the target, and calculated on a pixel grid of 0.05 m cross-track by 0.1 m along-track, covering an area of 6.4 m by 6.4 m.
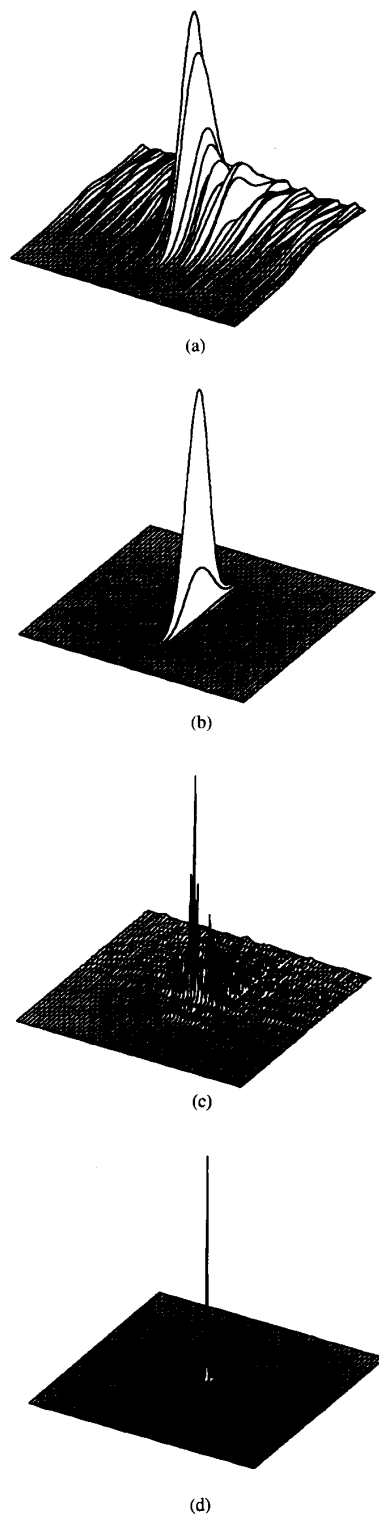
Fig. 4. The intensity distribution formed by combining all 20 narrow-band images both noncoherently, (a) real data, (b) simulated data, and coherently for (c) real data, and (d) simulated data. All image distributions are centered on the target and are calculated on a pixel grid of 0.05 m cross-track by 0.1 m along-track, covering an area of 6.4 m by 6.4 m.

VI. DISCUSSION

Images produced by highly coherent systems suffer from the undesirable property of a speckly appearance, where there are bright and dark areas in the image that are of the same order of size as the details of the object being imaged. These bright and dark areas are not related to any details of the object being imaged, and therefore, speckle degrades the image quality and resolution.

To reduce the effect of speckle, the speckly image can be smoothed using a low-pass spatial, or alternatively, since speckle is not found with incoherent illumination, speckle effects can be reduced by using some form of noncoherent averaging in the production of the image. Both spatial compounding and frequency compounding have been used to reduce the effects of speckle. With spatial compounding, statistically independent echoes from different views are combined. This is a common technique in SAR and is called multilook processing [37], [38]. The full synthetic aperture is divided into a number of shorter subapertures and the images reconstructed from each of these subapertures and then noncoherently summed together. The resultant image has a poorer along-track resolution than an image produced using the full synthetic aperture, but the coherent speckle is reduced, producing a higher quality image.

Frequency compounding uses different transmitted frequencies [39] or splits a wide bandwidth signal into narrower frequency band [40], [41]. The result of these techniques is to improve the image contrast (reduce the speckle) by a factor $\sqrt{N}$, where N is the number of independent echoes compounded. However, frequency compounding, like spatial compounding, results in a loss of resolution due to the requirement that the compounded echoes be uncorrelated.

The speckle reduction techniques described above are only applicable to speckle resulting from coherent illumination of a rough object. If the speckle is generated by medium turbulence, however, then compounding leads to a blurred image. This type of speckle is a result of a convolution of the desired object with a noisy point spread function, and is produced in both coherent and incoherent imaging systems. Deconvolution techniques are therefore required to reduce this form of image speckle, and in particular blind deconvolution, since the noisy point spread function is generally unknown [42].

The performance of a coherent synthetic aperture sonar is also limited by the phase accuracy of the received signals. The phase errors in sonar can be split into three categories; medium, platform, and hardware dependent phase errors. The hardware dependent phase errors result from timing errors, and phase shifts through analog filters in the receiver. The effect of repeatable frequency-dependent phase shifts due to the medium or receiver electronics is to disperse the echo signals and thus degrade the range resolution capability of the sonar. Provided the phase shifts are predictable, and do not vary too greatly with temperature, they can be corrected using lookup tables. Where the phase accuracy is of great importance, the demodulation/correlation of the echo signals should be implemented using digital signal processing techniques.

The medium dependent phase errors result from acoustic path length variations due to inhomogeneities in the medium. These path length fluctuations produce greater phase errors at the higher frequency components of the echo signals and are the limiting factor in the performance of coherent imaging.

Finally, the biggest impairment to synthetic aperture experimentation has been the lack of accurate monitoring of the platform trajectory. Although motion compensation is routinely applied to SAR imaging, the longer integration times required by the sonar counterpart necessitate more accurate platform monitoring. In SAR systems, platform navigation can also be supplemented by alignment based on the received signal itself. This process is called autofocusing [38], [43]. Echoes from a target highlight (natural or artificial—e.g., a beacon) are aligned and then the range rate of other features relative to the highlight is calculated. From this it is possible to deduce the deviation from a straight path [10], [44], [45]. Although primarily suited to spotlight mode SAR [46], similar techniques may be useful in synthetic aperture sonar imaging. For example, consider a sonar imaging to both port and starboard. Any deviation from a straight track causes the echoes from one side to be shifted up in Doppler while echoes from the other side are shifted down in Doppler. Providing that there are suitably strong reflectors on both sides of the sonar, it may be possible to determine the rate of displacement from the target Doppler histories. Similarly, correlating echoes forward and aft of the sonar may be useful for determining platform yaw.

There are many conflicting factors that influence the choice of the optimum operating parameters for a synthetic aperture sonar. The best performance is obtained if the real aperture is increased as far as possible, consistent with the desired along-track resolution [9]. Reducing the length of the real aperture increases the signal processing and data storage requirements. In addition, the Doppler bandwidth is also increased, which may require the prf to be increased to ensure adequate sampling, thus reducing the unambiguous range—albeit by a small amount in most sonar applications.

The choice of operating frequency is more difficult. Table II summarizes the frequency dependence of some of the more important factors. It is not immediately obvious, however, what the optimum operating frequency of a synthetic aperture sonar should be. For instance, increasing the operating frequency makes the sonar more susceptible to path length errors, but by the same token, the synthetic apertures are now shorter, thereby easing coherence difficulties. Surprisingly, higher frequency operation is less susceptible to platform speed errors. Although the wavelength is shorter, and less tolerant of path length errors, increasing the frequency reduces the beamwidth (assuming a fixed transducer size), and therefore, it would seem that the tolerance to a speed error would be independent of frequency. However, the phase error is proportional to the square of the integration time, and thus also to the square of the beamwidth. Therefore, the overall result of increasing the frequency is a higher tolerance to platform speed errors [8]. Theory suggests, however, that a synthetic aperture sonar can give a comparable performance to a nonsynthetic aperture sonar but at a lower frequency [19], [47].

1.....111111111111111111111111

[26] R. J. Urick, *Principles of Underwater Sound*. New York: Mc-Graw Hill, 2nd ed., 1975.

[27] W. C. Knight, R. C. Pridham, and S. M. Kay, "Digital signal processing for sonar," *Proc. IEEE*, vol. 69, pp. 1451-1507, Nov. 1981.

[28] J. H. Tarng and C. C. Yang, "Effects of propagation on the operation of a synthetic aperture sonar," *J. Acoust. Soc. Am.*, vol. 82, pp. 1403-1408, Oct. 1987.

[29] M. Sack, M. R. Ito, and I. G. Cumming, "Application of efficient linear FM matched filtering algorithms to synthetic aperture radar processing," *Proc. Inst. Elec. Eng.*, vol. 132, Part F, pp. 45-57, Feb. 1985.

[30] R. P. Perry and L. W. Martinson, "Radar matched filtering," in *Radar Technology*, E. Brookner, Ed. Dedham, MA: Artech House Inc., 1978, ch. 11.

[31] K. Nagai, "Multifrequency acoustic holography using a narrow pulse," *IEEE Trans. Sonics Ultrason.*, vol. SU-31, pp. 151-156, May 1984.

[32] P. de Heering, "Alternate schemes in synthetic aperture sonar processing," *IEEE J. Oceanic Eng.*, vol. OE-9, pp. 277-280, Oct. 1984.

[33] P. D. Hanstead, "Simplified digital synthesis of ultrasonic images," in *Proc. Roy. Soc. A*, vol. A 374, pp. 491-502, 1981.

[34] D. J. Wingham, "Square-law detected synthetic aperture radar," *Electronics Letters*, vol. 24, pp. 419-421, Mar. 1988.

[35] P. T. Gough, "Side-looking sonar or radar using phase difference monopulse techniques; coherent and noncoherent applications," *Proc. Inst. Elec. Eng.*, vol. 130, Part F, pp. 392-398, Aug. 1983.

[36] A. de Roos, J. J. Sinton, P. T. Gough, W. K. Kennedy, and M. J. Cusdin, "The detection and classification of objects lying on the seafloor," *J. Acoust. Soc. Am.*, vol. 84, pp. 1456-1477, Oct. 1989.

[37] W. J. vande Lindt, "Digital technique for generating synthetic aperture radar images," *IBM J. Resource Development*, vol. 20, pp. 415-432, Sept. 1977.

[38] J. C. Kirk, Jr., "A discussion of digital processing in synthetic aperture radar," *IEEE Trans. Aerosp. Electronic Syst.*, vol. AES-11, pp. 326-337, May 1975.

[39] P. A. Magnin, O. T. von Ramm, and F. L. Thurstone, "Frequency compounding for speckle contrast reduction in phased array imaging," *Ultrasonic Imaging*, vol. 4, pp. 267-281, July 1982.

[40] R. H. T. Bates and B. S. Robinson, "Ultrasonic transmission speckle imaging," *Ultrasonic Imaging*, vol. 3, pp. 378-394, Oct. 1981.

[41] V. L. Newhouse, N. M. Bilgutay, J. Saniie, and E. S. Furgason, "Flaw-to-grain echo enhancement split-spectrum processing," *Ultrasonics*, vol. 20, pp. 59-68, Mar. 1982.

[42] R. H. T. Bates and M. J. McDonnell, *Image Restoration and Reconstruction*. Oxford: Clarendon Press, 1986.

[43] J. C. Kirk, Jr., "Motion compensation for synthetic aperture radar," *IEEE Trans. Aerosp. Electronic Syst.*, vol. AES-11, pp. 338-348, May 1975.

[44] A. B. E. Ellis, "A proposed method of digitally processing SAR data from a satellite," in *Proc. Int. Conf. Radar - Present and Future*, pp. 155-160, Institution of Electrical Engineers, 1973.

[45] M. R. Vant, "A spatially-variant autofocus technique for synthetic-aperture radar," in *Radar 82 - Proc. Int. Conf.*, pp. 159-163, Institution of Electrical Engineers, 1982.

[46] D. Blacknell and R. G. White, "Prediction of the geometric positioning errors in SAR imagery," in *Radar 87: Proc. Int. Conf.*, pp. 68-72, Institution of Electrical Engineers, 1987.

[47] L. J. Cutrona, "Additional characteristics of synthetic-aperture sonar systems and a further comparison with nonsynthetic-aperture sonar systems," *J. Acoust. Soc. Am.*, vol. 61, pp. 1213-1217, May 1977.

Michael P. Hayes received the BE degree (electrical and electronic engineering) in 1985 and the Ph.D. in 1990 from the University of Canterbury, Christchurch, New Zealand.

Since then he has worked as a self-employed consultant in acoustics and signal processing.
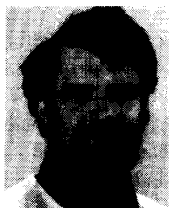
Peter T. Gough received the B.E. and Ph.D. in electrical engineering at the University of Canterbury in 1970 and 1974, respectively.

He spent three years at The Institute of Optics at the University of Rochester, New York and two further years at the University of Manitoba. He returned to New Zealand in 1980 to take up a position in the Electrical and Electronic Engineering Department, University of Canterbury, where he is now Head of the department.

Dr. Gough is a Fellow of the Institution of Professional Engineers of New Zealand.